MICRO-PIV CHARACTERIZATION OF LAMINAR DEVELOPED FLOWS OF NEWTONIAN AND NON-NEWTONIAN FLUIDS IN A SLIT CHANNEL

Carlos Completo*, Vitor Geraldes*, Viriato Semião**

Comprehensive knowledge of hydrodynamics inside the feeding channels of spiral-wound membrane modules is recognized as crucial for the efficient operation of such separation equipments. Slits are laboratory models widely used to mimic the fundamentals of hydrodynamics and mass transfer in spiral-wound membrane modules. In this work micro-PIV was the technique chosen to characterize fully developed laminar flows in a slit for both Newtonian and non-Newtonian fluids. Experiments with water, water-glycerol and water-glycerol-xanthan were carried out at different flow rates, ranging from 4.3 to 25.3 L/h. The ternary mixture water-glycerol-xanthan simulates the non-Newtonian rheological behavior of blood. The other fluids are Newtonian and exhibit different viscosities. The fluids rheology was characterized making recourse to a viscometer. Using micro-PIV, velocity maps at several depths of the channel were obtained. As expected, results showed that the Newtonian fluids flows exhibit parabolic profiles typical of laminar developed flows in slits. On the other hand, slightly flattened profiles characterize the non-Newtonian fluid flows. Comparisons with the analytical solutions for laminar developed flows in rectangular slits are very encouraging.

Keywords : *micro-PIV, slit, channel, non-Newtonian, blood analogue, xanthan, laminar*

1. Introduction

Membrane separation technology is one of the used technologies in processes of water purification and concentration of solutions. The development of compact equipment, like spiral-wound modules, led to high ratios of transfer area per unit of volume allowing for high flow rates [1]. To increase mass transfer, minimizing simultaneously the concentration polarization and reducing fouling, structural spacers that modify the fluid flow behavior in an open channel have been used. However, the flow around these spacers induce an increase of the pressure drop making important the study and optimization of the system. Spiral-wound modules have been traditionally modeled using flat channels known as *slits* [2–4].

The space between membranes in a spiral-wound module ranges from 1.2 to 2.0 mm and, despite the applicability of the continuum approach, the available experimental results refer mainly to flow bulk properties (as, for example, pressure). In this work, velocity profiles of flows inside a slit channel, for both Newtonian and non-Newtonian fluids, are obtained. This complements a previous work [3] that performed a detailed study of pressure drops in the

* C. Completo, V. Geraldes, Chemical and Biological Engineering Department, Instituto Superior Técnico, 1049-001 Lisboa, Portugal
** V. Semião, Mechanical Engineering Department, Instituto Superior Técnico, 1049-001 Lisboa, Portugal

same slit. The used Newtonian fluids were deionized water and a water-glycerol mixture. As non-Newtonian fluid a ternary mixture of water-glycerol-xanthan gum that mimics the rheological behavior of blood was utilized.

Human and animal bloods used as working fluids in some other experiments [5–6] exhibit specific characteristics (no transparency, large variability and problems with cleaning the devices) that limit their applicability for laboratory experiments, particularly for those with optical devices. Due to these reasons blood has been replaced by other fluids, blood analogues, like the one used herein, a mixture of water, glycerol and xanthan gum [7].

Xanthan gum is a natural polysaccharide produced by bacteria of the genus *Xanthomonas*, and usually are used strains of *Xanthomonas campestris* [8].

For steady, incompressible and developed laminar flows of Newtonian fluids in pipes and in channels of rectangular, triangular, trapezoidal and elliptical cross section, analytical solutions described elsewhere [9–10] exist. For the particular case of a rectangular channel (slit) with the geometry defined in Figure 1, the velocity profile $v_{x}(y, z)$ with the no-slip boundary condition at the walls, is expressed by:

$$v_x(y,z) = \frac{48\,Q}{\pi^3\,W\,H} \frac{\displaystyle\sum_{i=\text{odd}}^{\infty} \frac{1}{i^3}\left[1 - \frac{\cosh\!\left(i\,\pi\,\frac{y}{H}\right)}{\cosh\!\left(i\,\pi\,\frac{W}{2\,H}\right)}\right]\sin\!\left(i\,\pi\,\frac{z}{H}\right)}{1 - \displaystyle\sum_{i=\text{odd}}^{\infty}\frac{1}{i^5}\,\frac{192\,H}{\pi^5\,5}\,\tanh\!\left(i\,\pi\,\frac{W}{2\,H}\right)}\ , \tag{1}$$

where Q is the volumetric flow rate, H and W are, respectively, the height and width of the channel.
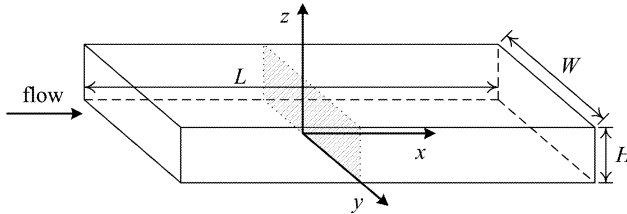

Fig.1: Slit geometry and coordinate system of the
analytical solution given by equation (1)

Although the previous analytical solutions exist, experimental techniques to determine the velocity profiles are essential to characterize flows in more complex geometries. There are several non-intrusive techniques like Laser Doppler Velocimetry (LDV), Particle Image Velocimetry (PIV), Scalar Image Velocimetry (SIV) and techniques based on Nuclear Magnetic Resonance (NMR) [11–12].

Micro-PIV, the technique used in this work to measure the velocity field and described below in detail, is an adaptation of PIV to micro-scale.

In the literature several works using the micro-PIV technique to study the fluid flow in square and rectangular micro-channels can be found [10, 13–18]. In all these studies there is good agreement between experimental velocity profiles and theoretical/numeric previsions, especially at the central region of the channel. Near the walls the deviation can be considerable and many physical effects may contribute to this behavior (wall slip,

electrophorectic motion, electrostatic repulsion [10]). None of the previous studies were performed in slits with geometry similar to those used in this work.

2. Experimental

2.1. Materials, sample preparation and equipment

The working fluids were prepared with deionised water, glycerol (bidistilled at 99.5 % batch 09J290503 from BDH PROLABO) and edible xanthan gum (batch 8080909 from MyProtein.co.uk).

The tracer particles used were fluorescent polystyrene spheres with an average diameter of $1\,\mu$m (red nile FluoSpheres carboxylate-modified microspheres from Invitrogen, lots 32086W and 649959). In the samples prepared for the micro-PIV experiments the water weight was adjusted to account for the addition of the tracer particles suspension ($6\,$mL/L).

Water and glycerol are easily miscible and were mixed with manual stirring. The mixture of water, glycerol (35 % w/w) and xanthan gum (0.02 % w/w) was produced with magnetic stirring over 12 hours to obtain a clear fluid [8]. The obtained mixtures were named as follows: WGggXxxx where 'W' stands for water, 'Ggg' stands for glycerol with a 'gg' mass percentage and 'Xxxx' stands for xanthan with x.xx mass percentage.

The rheological measurements of the mixtures without tracer particles were performed in a cone-plate viscometer (LVDV-II+ model with CPE-40 cone from Brookfield) using the Rheocalc software (version 3.2) for data acquisition. The temperature was controlled with a thermostatic bath (VC3 controller from Julabo).
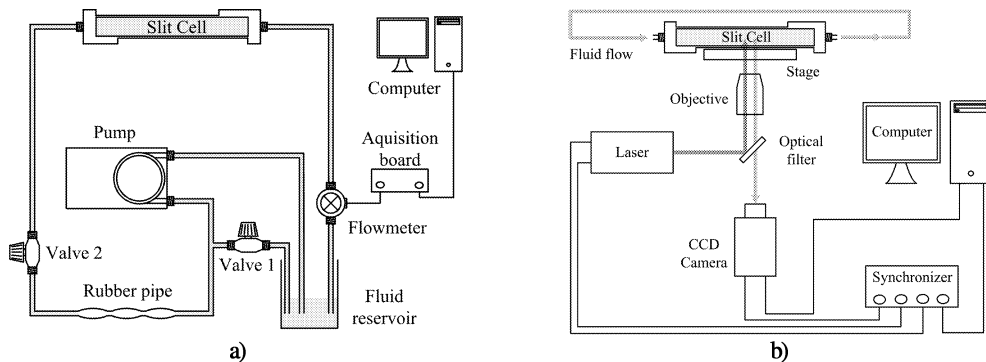

Fig.2: The experimental rig: a) hydraulic circuit; b) micro-PIV system

The cell containing the slit is integrated in a hydraulic circuit (Figure 2a) and is mounted on the microscope stage. The slit designed with 30 mm wide, 200 mm long and 1.2 mm height was built with smooth PMMA walls.

The working fluid flows in the hydraulic circuit driven by a peristaltic pump (LAV 200 model from Dosiper). The flow rate is controlled with two manual valves and data are acquired from a flowmeter (SCAU-010A from ELAB) through an acquisition board (NI USB-6008 from National Instruments) using a Labview program. The pulses of the flow due to the pump are damped passing in a rubber pipe with clamps.

In the experiments with water the used flow rates were 4.4, 8.4, 12.7, 17.6 and 22.8 L/h while for the other fluids the flow rates used were 6.7, 11.3, 16.0, 20.6 and 25.3 L/h.

The used micro-PIV hardware consists of six main parts: a pulsed Nd:YAG laser emitter (Solo II-15 from New Wave Research); an inverted microscope (DM ILM from Leica Microsystems); an optical filter (Y3 cube filter from Leica Microsystems); a CCD camera (Flowsense 2M from Dantec); a synchronizer and a computer (Figure 2b). The scale factor of the used lens (HI PLAN 10×, from Leica Microsystems – catalogue number 506228) was determined (0.100323) using a micrometric stage ruler (MBM13100 from Nikon).

2.2. Methods and data treatment

Particle Image Velocimetry (PIV) was developed in the 1980s [19] and the studies with micro-PIV, the technique used in this work, started after the pioneer work of Santiago et al. [20] who studied the fluid flow around a cylinder with a diameter of $30\,\mu m$. Both techniques are based on determining the velocity of the fluid, v, at an area of observation by obtaining the displacement of patterns of tracer particles, Δl, in a given known time interval, Δt:

$$v = \frac{\Delta l}{\Delta t} \ . \tag{2}$$

The two-dimensional displacement of the pattern is determined taking two images (frames) of the flow with a Δt delay and using signal processing within interrogation areas (Figure 3).
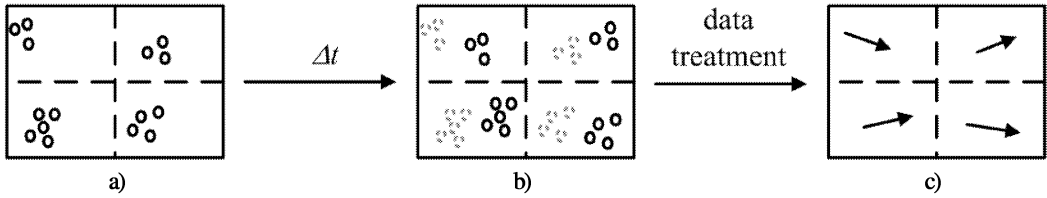

Fig.3: *Scheme of obtaining vector maps with micro-PIV: a) image at $t = t_0$;*
b) image at $t = t_0 + \Delta t$; c) vector map after data treatment

The main difference between a micro-PIV and a conventional PIV system is the illumination of the flow under study. For PIV systems illumination is a sheet of laser light, being the depth of focus determined by the width of such sheet. It is nearly impossible to produce sheets of light with adequate thickness (1–10 micrometers [21]) for microscale studies. Therefore, in micro-PIV the light illuminates the entire volume and the depth-of-field, δ_z, is determined by the characteristics of the used lens and is defined by [22]:

$$\delta_z = \frac{n\,\lambda}{(NA)^2} + \frac{n\,e}{(NA)\,M} \ , \tag{3}$$

where n is the refractive index of the medium, λ is the wavelength of the light, NA is the numeric aperture of the lens, e is the pixel size of the CCD camera being used and M is the magnification of the lens. However, the light emitted by tracer particles located out of focus can influence the signal processing. To account for this contribution the depth of correlation, δ_{DOC}, was defined [23]:

$$\delta_{DOC} = 2 \left[\frac{1 - \sqrt{\varepsilon}}{\sqrt{\varepsilon}} \left(f_\#^2\, d_p^2 + \frac{5.95\,(M+1)^2\,\lambda^2\,f_\#^4}{M^2} \right) \right]^{\frac{1}{2}} \ . \tag{4}$$

In the previous equation $f_\#$ is the focal number of the lens ($f_\# = 0.5\sqrt{(n/NA)^2 - 1}$ [22]), d_p is the particle diameter and ε is the relative threshold below which the defocused particle images have no significant influence.

Micro-PIV technique allows for obtaining two dimensional velocity vector maps by using signal processing algorithms. The fundamental one is the cross-correlation algorithm that uses only one pair of frames [24]. To improve the signal-to-noise ratio, in steady state flows, the average correlation algorithm (also known as ensemble algorithm), which determines the vector map based on the average correlation of several pairs of frames [25] can be used.

Another issue that should be kept in mind is that the displacement of the objective results in different displacements of the focal plane, according to the immersion and walls media [26]. If the focal plane is always in the fluid channel its displacement, Δz_dfp, can be determined by:

$$\Delta z_\mathrm{dfp} = \alpha\,\Delta z_\mathrm{do}\;. \tag{5}$$

In equation 5 Δz_do is the displacement of the objective and α is calculated by:

$$\alpha = \sqrt{\frac{n_\mathrm{i}^2 - (n_0\,\sin\theta_0)^2}{n_0^2 - (n_0\,\sin\theta_0)^2}}\;, \tag{6}$$

where n_0 and n_i are, respectively, the refractive index of the immersion medium of the objectives and of the working fluid, θ_o is the aperture angle of lens in its immersion medium and can be estimated by $NA = n\sin\theta$ [22].

The micro-PIV measurements were performed mainly by using the lateral access in several vertical planes, at $14\,\mathrm{cm}$ from the slit entrance (Figure 4). For the measurements with water and water-glycerol it was possible to reach $3\,\mathrm{mm}$ in depth (from lateral wall). However, with water-glycerol-xanthan the maximum depth possible to attain with the lens mentioned above was $1.5\,\mathrm{mm}$. When accessing the slit by the top wall, measurements at half channel width of the slit were made also at $14\,\mathrm{cm}$ from the slit entrance (Figure 4).
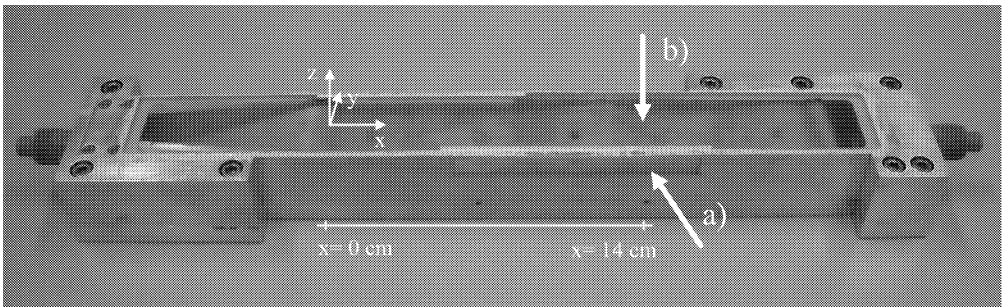

Fig.4: Locations of the micro-PIV measurements: a) lateral access; b) top access

The depth of correlation for the used lens, calculated using equation 4, is $61\,\mu\mathrm{m}$. For the measurements performed by the lateral access the minimum objective step between consecutive planes, Δz_do, was $40\,\mu\mathrm{m}$ near the wall. Using this value and equation 5 we estimate the minimum displacement of the focal plane, Δz_dfp, as $54\,\mu\mathrm{m}$. Hence, the effects of the small overlap between measuring planes is not relevant. Measurements made through the top wall access, for WG35X002, were performed with an objective displacement of $20\,\mu\mathrm{m}$ to try to define a good velocity profile and, therefore, overlapping was higher.

Data acquisition and post-treatment was done with DynamicStudio software (version 2.30.47 from Dantec). The adopted number of pairs of images for each vector map was 100 and the time delay between laser pulses was adjusted according the depth of focus plane in the channel, in such a way that the displacements of the tracer particles did not exceed 25 % of the interrogation area dimension [24].

The interrogation areas have sizes of 64×64 pixels on the planes near the wall, up to 1500 μm, and 128×128 pixels at larger distances. With this setup the spatial resolutions are 47.4×47.4 μm^2 and 94.7×94.7 μm^2, respectively.

3. Results and discussion

3.1. Characterization of the fluids

The rheological characteristics of several fluids (water, WG35, WG52 and WG35X002) were determined at 30 °C.

The viscosities of the Newtonian fluids, presented in Table 1, were determined by the slope of shear stress versus shear rate plot and, as expected, the determination coefficient of the fitted linear relationship, R^2, was close to unity (≥ 0.999). The present experimental results fit very well other authors correlation [27] with deviations smaller than 2.9 %.

Fluid	Experimental	Literature [27]	Deviation (%)
Water	0.804	0.800	0.5
WG35	2.285	2.221	2.9
WG52	4.650	4.669	−0.4

Tab.1: Viscosity (cP) of some Newtonian fluids at 30°C

The used non-Newtonian fluid, a mixture of water-glycerol-xanthan, presents a pseudo-plastic behavior that can be seen in Figure 5.

With this result we confirmed that the used non-Newtonian fluid mimics reasonably the blood viscosity. The very low concentration of the tracer particle does not influence the rheological results according to the Einstein rule [29].
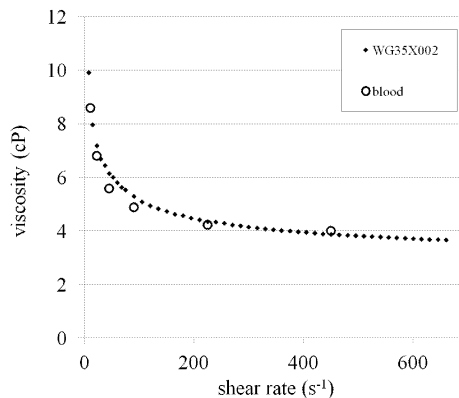

Fig.5: Viscosity as function of shear rate for blood [28] (open symbol)
and water-glycerol-xanthan mixture (black symbol) at 30°C

3.2. Characterization of the flows

One of the requirements of the micro-PIV technique is that the tracer particles should follow the streamlines without slip. A simple way to check this imposition is the comparison between the response time of the particle and smallest time scale in the flow, [22]. Due to the small size of the tracer particles and its density the response time in the three fluids (magnitude of $6{\times}10^{-8}$ s for water and $1{\times}10^{-8}$ s for WG52) are negligible compared to the characteristic time scale of the flow, defined by the time interval between two consecutive laser pulses (magnitude between of $4{\times}10^{-5}$ and $5{\times}10^{-4}$ s).

Figure 6 shows a frame taken with the micro-PIV system and the velocity map obtained after data acquisition and treatment with DynamicStudio software. This acquisition was obtained in a vertical plane through the lateral access (see Figure 4a).
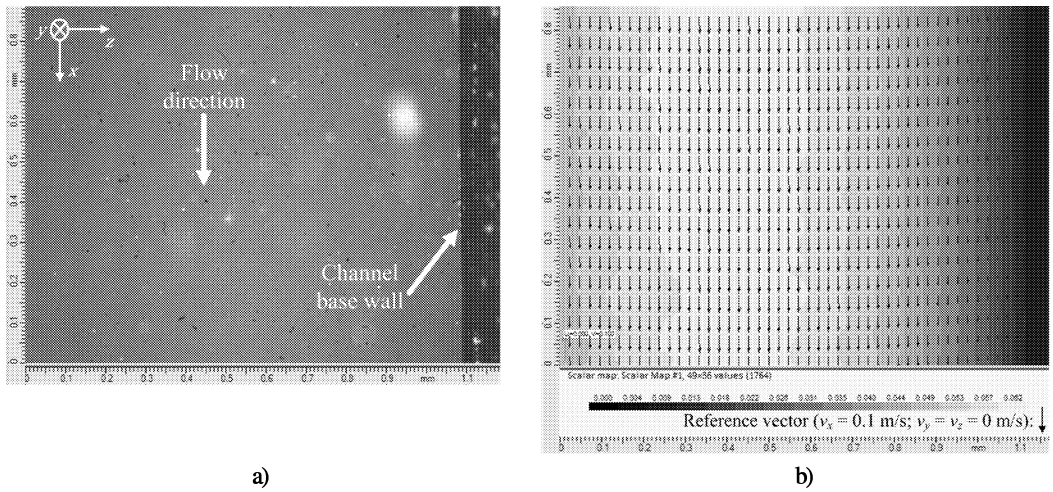

a)   b)

Fig.6: *Micro-PIV results: a) Channel overview; b) 2D velocity vector map obtained, in a vertical plane, at a distance of 0.171 mm from lateral wall for WG52 flow (Q = 20.6 L/h)*

Figure 7 displays the non-dimensional measured velocity profiles at half width of the channel for different fluids. The dimensionless velocity and dimensionless height, v_{x}^* and h^*, are defined as:

$$v_{\mathrm{x}}^* = \frac{v_{\mathrm{x}}}{v_{\mathrm{x,pm}}} \ , \tag{7}$$

$$h^* = \frac{z}{H} \ , \tag{8}$$

where v_{x} and $v_{\mathrm{x,pm}}$ are respectively the velocity at height z and the maximum velocity of the fitted parabola to the velocity profile both in x direction.

We can consider that Newtonian fluids flows in the studied region of the slit are developed and therefore, when the velocity profiles, at the same location, are plotted in a non-dimensional coordinate system, they coincide (see Figures 7a and 7b). In fact, since the maximum entrance length is 2.3 cm [30–33] and occurs for the higher Reynolds number flow with water studied herein, measurements were performed quite downstream that value.
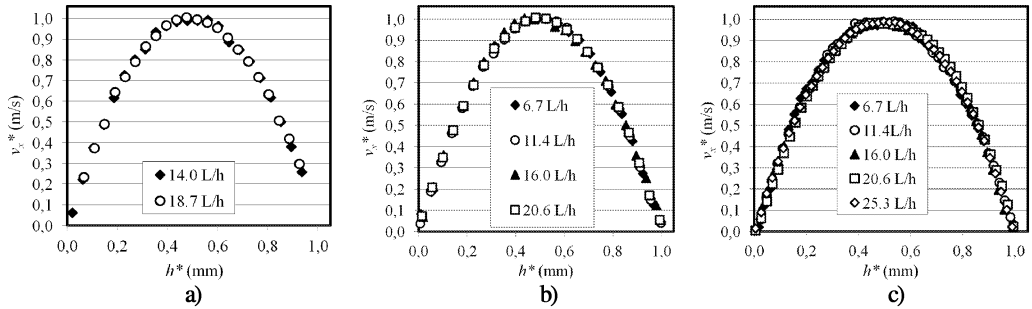
Fig.7: *Dimensionless velocity profiles, at half width of the channel, obtained with: a) water; b) WG52; c) WG35X002*

From Figure 7c we can also see that the profile of the non-Newtonian fluid is slightly flattened at the center when compared with the parabolic one for Newtonian fluids. This result is in agreement with other authors conclusions [34].

The maximum values of v^* are between 0.995 and 1.006 for the water profiles, between 1.002 and 1.008 for WG52, and between 0.982 and 0.991 for WG35X002.

Putting together the measured velocity profiles at several depths one can reconstruct the three dimensional flow field. Figure 8 shows two cases of the 3D reconstruction of the flow for WG35X002 up to a depth, from the lateral wall, of about 1.5 mm.

As expected, the velocity approaches zero close to the wall, due to the no-slip boundary condition, and exhibits the characteristic parabolic shape of laminar developed flows of Newtonian fluid in a rectangular channel (given by equation 1).

Figure 9a shows the velocity profiles of the WG52 and WG35X002 flows, at half height of the channel as a function of the channel width (starting at the lateral wall). Each point stands for the maximum velocity at the corresponding measurement plane (see Figure 8). The solid lines are the analytical velocities values, computed with equation 1, using the experimental flow rates of the measurements with WG52 and assuming that the channel has a height of 1.34 mm. This channel height corresponds to the average of the distances between the roots of the parabolas fitted to velocity profiles of WG52 at half width of the channel.
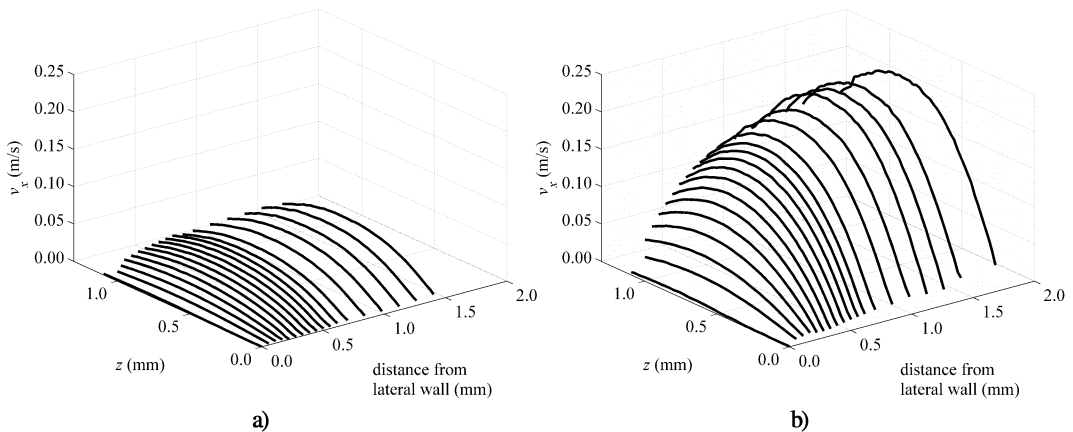

Fig.8: *Three-dimensional reconstruction of the velocity profiles obtained with WG52 for: a) $Q = 6.7\,L/h$; b) $Q = 25.3\,L/h$*

From this figure we can see that the velocity profiles have a good shape agreement with the analytical solution despite numerical deviations in the absolute values. For instance, at a depth of 2 mm the analytical values are in excess to the corresponding experimental ones with deviations of 10.0 to 15.3 %.

Similarly, and although not displayed herein, the deviations in the case of water were, at a depth of 2 mm from lateral access, between -0.9 and 16.7 %.

The cell was designed to allow for height changes of the slit channel. The objective, in the present work, is to study the flows in a slit with a design height of 1.2 mm. However, as said before, the estimated height of the channel slit is 1.34 mm which is higher than the design value.

These observations lead us to admit that there are significant uncertainties in slit height. In fact, if equation 1 is computed for a channel height of 1.45 mm experimental results and analytical solutions are much closer exhibiting deviations ranging from 1.9 to 7.7 %, at $y = 2$ mm, as shown in Figure 9b. Another possible cause of such deviations is an erroneous calibration of the flowmeter leading to smaller flow rates than those expected.
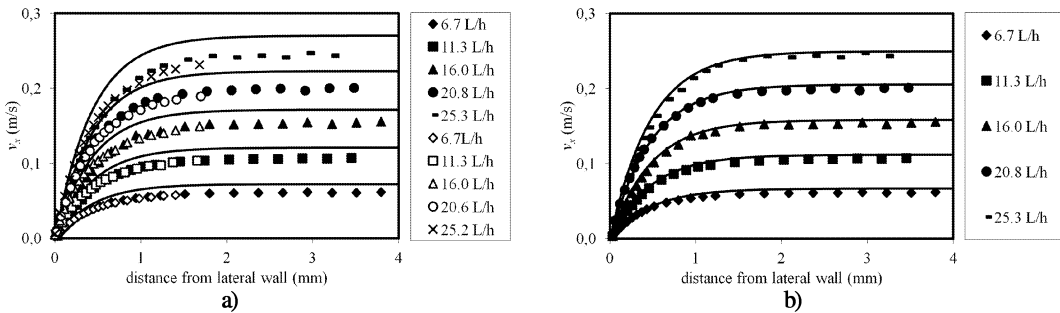

Fig.9: *Comparison of experimental and analytical velocity profiles at half height of the channel; the closed and $-$ symbols stands for the experimental WG52 flows; the open and $\times$ symbols represents the experimental WG35X002 flows; lines are the analytical values given by equation (1) and calculated with : a) height $= 1.34$ mm; b) height $= 1.45$ mm*

4. Conclusions

In this work distinct velocity profiles of Newtonian and non-Newtonian fluids flowing through an open slit channel with smooth walls were measured. The design dimensions of the slit are 1.2 mm in height and a sectional cross area of 30×200 mm^2. As Newtonian fluids water and a water-glycerol (52 % w/w) mixture are used. As non-Newtonian fluid it is used a mixture of water, glycerol (35 %) and xanthan gum (0.02 %).

The experimental results confirmed that the velocity profiles for Newtonian fluids flows are parabolic in the vertical planes of the channel, and exhibit good agreement in shape with the analytical solution for the developed laminar flow in rectangular channel. For the non-Newtonian fluid the velocity profiles are slightly flattened at the central region of the channel.

The micro-PIV proved to be a suitable technique to characterize the velocity profiles experimentally up to $1.0 - 1.5$ mm from the nearest wall with lens used $(10\times)$, since a high enough signal to noise ratio at fair spatial resolution $(47.4 \times 47.4 \,\mu\text{m}^2)$ can be obtained.

Acknowledgements

References

[1] Doyen W.: Latest developments in ultrafiltration for large-scale drinking water applications; Desalination, 113, 165–177, (1997)

[2] Ranade V., Kumar A.: Fluid dynamics of spacer filled rectangular and curvilinear channels; Journal of Membrane Science, 271, 1–15, (2006)

[3] Almeida A., Geraldes V., Semião V.: Microflow hydrodynamics in slits : Effects of the walls relative roughness and spacer inter-Filaments distance, Chemical Engineering Science, 65, 3660–3670, (2010)

[4] Geraldes V., Semião V., Pinho M.N.: Flow management in nanofiltration spiral wound modules with ladder-type spacers, Journal of Membrane Science, 203, 87–102, (2002)

[5] Lima R., Wada S., Tanaka S., Takeda M., Ishikawa T., Tsubota K., Imai Y., Yamaguchi T.: In vitro blood flow in a rectangular PDMS microchannel : experimental observations using a confocal micro-PIV system, Biomedical Microdevices, 10, 153–167, (2008)

[6] Lee J.Y., Ji H.S., Lee S.J.: Micro-PIV measurements of blood flow in extraembryonic blood vessels of chicken embryos, Physiological Measurement, 28, 1149–1162, (2007)

[7] Brookshier K.A., Tarbell J.M.: Evaluation of a Transparent Blood Analog Fluid – Aqueous Xanthan Gum Glycerins, Biorheology, 30(2), 107–116, (1993)

[8] Song K.-W., Kim Y.-S., Chang G.-S.: Rheology of Concentrated Xanthan Gum Solutions : Steady Shear Flow Behavior, Fibers and Polymers, 7(2), 129–138, (2006)

[9] Shaj R.K., London A.L.: Advances in Heat Transfer – Supplement 1 – Laminar Flow Forced Convection in Ducts : a Source Book for Compact Heat Exchanger Analytical data, Academic Press, (1978)

[10] Zheng X., Silber-Li Z.: Measurement of velocity profiles in a rectangular microchannel with aspect ratio $\alpha = 0.35$, Experiments in Fluids, 44, 951–959, (2008)

[11] Meinhart C.D., Wereley S.T., Santiago J.G., Micron-Resolution Velocimetry Techniques, Laser techniques applied to fluid mechanics : selected papers from the 9th international symposium; Springer, 2000

[12] Han S.-I., Marseille O., Gehlen C., Blümich B.: Rheology of Blood by NMR, Journal of Magnetic Resonance 152, 87–94, (2001)

[13] Devasenathipathy S., Santiago J.G., Wereley S.T., Meinhart C.D., Takehara K.: Particle imaging techniques for microfabricated fluidic systems, Experiments in Fluids, 34, 504–514, (2003)

[14] Wei X., Joshi Y.: Experimental and numerical study of sidewall profile effects on flow and heat transfer inside microchannels, International Journal of Heat and Mass Transfer, 50, 4640–4651, (2007)

[15] Wang H., Wangb Y.: Measurement of water flow rate in microchannels based on the microfluidic particle image velocimetry, Measurement, 42, 119–126, (2009)

[16] Wiber W., Ehrhard P.: Experiments on the Laminar/Turbulent Transition of Liquid Flows in Rectangular, Microchannels Heat Transfer Engineering, 30(1–2), 70–77, (2009)

[17] Ahmad T., Hassan I.: Experimental Analysis of Microchannel Entrance Length Characteristics Using Microparticle Image Velocimetry, Journal of Fluids Engineering 132, 041102, (2010)

[18] Silva G., Leal N., Semião V.: Micro-PIV and CFD characterization of flows in a microchannel : Velocity profiles, surface roughness and Poiseuille numbers, International Journal of Heat and Fluid Flow, 29, 1211–1220, (2008)

[19] Adrian R.J.: Twenty years of particle image velocimetry, Experiments in Fluids, 39, 159–169, (2005)

[20] Santiago J.G., Wereley S.T., Meinhart C.D., Beebe D.J., Adrian R.J.: A particle image velocimetry system for microfluidics, Experiments in Fluids, 25, 316–319, (1998)

[21] Lee S.J., Kim S.: Advanced particle-based velocimetry techniques for microscale flows, Microfluidics and Nanofluidics, 6, 577–588, (2009)

[22] Raffel M.: Particle Image Velocimetry – A Pratical Guide, Springer-Verlag, (2007)

[23] Olsen M.G., Adrian R.J.: Out-of-focus effects on particle image visibility and correlation in microscopic particle image velocimetry, Experiments in Fluids, 29(Supplement 1), S166–S174, (2000)

[24] Prasad A.: Particle image velocimetry; Current Science, 79 (1), 51–60, (2000)

[25] Meinhart C., Wereley S.T., Santiago J.G.: A PIV Algorithm for Estimating Time-Averaged Velocity Fields, Journal of Fluids Engineering, 122(2), 285–289, (2000)

[26] Kim B.J., Liu Y.Z., Sung H.J.: Micro PIV measurement of two-fluid flow with different refractive indices, Measurement Science and Technology, 15, 1097–1103, (2004)

[27] Cheng N.-S.: Formula for the Viscosity of a Glycerol-Water Mixture; Industrial and Engineering Chemistry Research, 47, 3285–3288, (2008)

[28] Janela J.P.V.: Mathematical and numerical modeling in hemodynamics and hemorheology (PhD Thesis), Department of Mathematics, Instituto Superior Técnico, (2008)

[29] Batchelor G.K.: An introduction to fluid dynamic, Cambridge Mathematical Library, (2000)

[30] Chen R.-Y.: Flow in the entrance region at low Reynolds numbers; Journal of Fluids Engineering, 95(1), 153–158, (1973)

[31] Durst F.; Ray S., Ünsal B., Bayoumi O.A.: The Development Lengths of Laminar Pipe and Channel Flows, Journal of Fluids Engineering, 127(6), 1154–1160, (2005)

[32] Oak J.; Pence D.V.; Liburdy J.A.: Flow Development of Co-Flowing Streams in Rectangular Micro-Channels, Microscale Thermophysical Engineering, 8, 111–128, (2004)

[33] Geraldes V., Semião V., Pinho M.N.: Nanofiltration Mass Transfer at the Entrance Region of a Slit Laminar Flow, Industrial & Engineering Chemistry Research, 37, 4792–4800, (1998)

[34] Shorten P.R., Wall D.J.N.: Fluid Velocity Profile Reconstruction for Non-Newtonian Shear Dispersive Flow, Journal of Applied Mathemathics and Decision Sciences, 5(2), 87–104, (2001)